Supporting Information

High-valence Mo doping for highly promoted water oxidation of NiFe (oxy)hydroxide

Liting Wei,[a] *Mingyue Du,*[a] *Rui Zhao,*[a] *Fei Lv,*[a] *Lubing Li,*[a] *Lei Zhang,*[a] *Di Zhou*[b] *and Jinzhan Su* *[a]

a. International Research Center for Renewable Energy & State Key Laboratory of Multiphase Flow in Power Engineering, Xi'an Jiaotong University, Xi'an Shaanxi 710049 (P.R.China)

b. Electronic Materials Research Laboratory, Key Laboratory of the Ministry of Education & International Center for Dielectric Research, School of Electronic and Information Engineering, Xi'an Jiaotong University, Xi'an 710049, Shaanxi, China

* Corresponding author at International Research Center for Renewable Energy & State Key Laboratory of Multiphase Flow in Power Engineering, Xi'an Jiaotong University, Xi'an Shaanxi 710049, P.R.China. E-mail: j.su@mail.xjtu.edu.cn

Experimental

Catalysts synthesis

The NiFeMo (loading amout:5.0mg/cm^2) catalyst were prepared via electrodeposition in a standard three-electrode configuration with CHI 760D electrochemical workstation. The nickel foam (NF, 1.0mm thickness, geometric area exposed to the solution: 1.0×1.0 cm^2) was used as the working electrode, Pt foil and Ag/AgCl electrode (1M KCl) served as the counter electrode and reference electrode, respectively. Before the electrodeposition, NF was cleaned in 3M HCl aqueous solution for 30 min to remove the oxide from the surface, followed by sonication in ethanol and deionized water for 10 min subsequently. Typically, 0.9 mmol $NiSO_4 \cdot 6H_2O$ (≥98.5, Sinopharm), 0.2 mmol $FeSO_4 \cdot 7H_2O$(≥99.0%,Sinopharm), and 0.1 mmol $Na_2MoO_4 \cdot 2H_2O$ (≥99.0%,Sinopharm) were dissolved in 20mL DI water as the electrodeposition electrolyte. Boric acid (≥99.5%,Sinopharm) and saccharin (≥99.0%,Sinopharm) were also added into this electrolyte to reach concentration of 40g L^{-1} and 1 g L^{-1}, respectively. The electrodeposition was conducted under a constant potential of -1.0V (vs. Ag/AgCl) for one hour. Afterward, the sample was carefully taken out from the electrolyte, rinsed with DI water, and dried in air (donated as NiFeMo/NF). In addition, we synthesize NiFeMo catalysts with different doping concentrations (15:4:1, 12:2:1, 6:1:1,12:1:2) by altering the ratio of Mo to Fe in the solution with keeping the total concentration of cation content and Ni content unchanged. Catalysts denoted as Ni, NiFe and NiMo were obtained by electrodeposition in the electrolytes with the absence of Fe, Mo ions, Mo ions or Fe ions in the electrolyte, respectively.

Material characterization

The phase compositions of the prepared samples were achieved using a X-ray diffraction (XRD) with Cu Kα radiation (λ=0.154nm) at 40kV and 40mA. The structural and morphological characterizations were obtained with a field-emission scanning electron microscope (SEM, JEOL JSM-7800F, Japan)

under an accelerating voltage of 3kV. and a transmission electron microscope (TEM, FEI Tecnai G2F30 S-Twin) equipped with energy dispersive x-ray spectrometer (EDS). X-ray photoelectron spectra (XPS) were acquired on a Kratos spectrometer (Axis Ultra DLD) with monochromatized Al Kα radiation (*hv*=1486.69eV), and the calibration of binding energy was performed with C1s peak at 284.8 eV.

Electrochemical Measurements

Electrochemical catalytic capability and other electrochemical properties were carried out in a three-electrode configuration in 1.0M KOH electrolyte with CHI 760D electrochemical workstation (Shanghai, China). The NF coated with electrocatalysts served as the working electrodes with a Pt foil (2cm×2cm) as the counter electrodes and Hg/HgO electrode as the reference electrodes, respectively. Before each electrochemical test, cyclic voltammetry (CV) from 0.9V to 1.8V at a scan rate of 100mV s^{-1} for 20 cycles were performed for the fresh sample in order to stabilize the catalyst' surface. Linear sweep voltammetry curves (LSVs) were obtained within a potential range from 1.0 to 1.8V versus reversible hydrogen electrode (RHE) at a sweep rate of 5mV/s. Electrochemical impedance spectroscope (EIS) was acquired at 1.5V versus RHE in a frequency range from 200 kHz to 50 mHz with an amplitude of 10mV. All polarization curves were obtained under 90% iR-compensation to exclude the ohmic losses of the solution. The electrochemically active specific area (ECSA) can accurately reflect the amount of active sites, which was estimated based on double-layer capacitance (C_{dl}). Briefly, the CVs within the non-Faradaic regions between 0.05 and 0.15V (vs. Hg/HgO) are recorded at different scan rates. By plotting capacitive current (j_{anodic}-$j_{cathodic}$)/2 at 0.1V (vs. Hg/HgO) against the sweep rate, a linear trend was obtained, and the C_{dl} value was given by the slope of the straight line. The ECSA can be obtained by the following formula:

$$ECSA = \frac{C_{dl}(Catalyst)}{C_s}$$

Where C_s is the specific capacitance with the value of 0.04 mF cm^{-2} for an ideal flat surface[1]

The temperature-dependent OER tests were performed at fixed temperatures from 10℃ to 50 ℃. The OER activation energy (Ea) was calculated by the Arrhenius relationship[2]:

$$\frac{\partial log j_k}{\partial T^{-1}} = -\frac{Ea}{2.3R}$$

where j_k is the kinetic current density, T is the absolute temperature, and R is the universal gas constant.

Turnover frequency (TOF) number specifying the extent of evolved oxygen gas per unit of time was gained by electrochemical measurements. To calculate Ni loading of cataysts, successive CV scans were performed at different scan rates from 2.5 to 15 mV s^{-1} in the potential range covering the oxidation and reduction potential of Ni (0.25-0.6 V vs Hg/HgO) in 1.0M KOH. The obtained slope from the linear regression of the recorded oxidation current responses versus scan rate gives the mole number of Ni active sites:

$$\text{Slope}=\frac{n^2F^2A\Gamma}{4RT}$$

in which *n* refers to the number of electrons transferred during the oxidation of Ni^{2+} to Ni^{3+} (n=1), *F* is the Faradic constant, A is the geometrical area of the electrode (1 cm^2), Γ is moles per unit area for Ni active sites (mol cm^{-2}), R and T represent the universal gas constant and absolute temperature, respectively. *m* is the number of moles for Ni on the surface participating in the OER and can be obtained by multiplying A by Γ.

$m=A\times\Gamma$

Afterwards, the TOF values based on Ni active sites were derived according to equation:

$$TOF = \frac{j\text{A}}{4Fm}$$

Where *j* is the current density (A cm^{-2}) of catalysts at a fixed overpotential, A is the surface area (1 cm^2), 4 indicates the four-electron transfer process in OER, *F* is the Faradic constant, and *m* presents Ni mole loading.

Faraday efficiency (FE) was evaluated by comparing the experimental gas production with the theoretical gas production. The FE was calculated by $FE=n_{ex}/n_{th}$, where n_{ex} is the produced moles of oxygen and n_{th} is the theoretical moles of oxygen. The experimental molars of gas can be calculated by $n_{ex}=V/V_m$, where V is volume of the measured gas and V_m is the molar volume. The volume of oxygen can be measured by the water drainage method. The theoretical moles of oxygen can be calculated by $N_{th}=Q/(n\times F)$, where Q(c) is total amount of electrical charge, F is Faradic constant (96485.3 C mol^{-1}), and n is 4 for oxygen.

Operando Raman Electrochemical Experiments

Operando Raman spectrum were acquired using a confocal HORIBA micro-Raman spectroscopy system with a 633 nm laser excitation. The acquisition time for different catalysts was 20 s with spectral range from 200 to 800 cm^{-1}. A three-electrode system consists of the NF deposited with NiFe and NiFeMo (oxy)hydroxides as working electrode, a Pt foil as counter electrode and a silver foil as quasi reference electrode (QRE), which was soaked in 1M KOH electrolyte. Setup and description are available in Figure S1. Because the operando Raman cell have specific geometry and limited space for a standard reference electrode, so an Ag foil was used as a quasi-reference electrode, which exhibit the same electrochemical behavior.[3-5] The potential-dependent in situ Raman spectra were recorded by sweeping the potential with a step of 0.1V and a settling time of 2 min.

Computational Methods

The Vienna Abinitio Simulation Package (VASP) based on Density functional theory (DFT) was employed in the entire calculations. [6-7] Spin polarization was taken into account. Perdew-Burke-Ernzerhof exchange-correlation functional within generalized gradient approximation was applied while a plane-wave basis set was implemented in the framework of the projector augmented wave (PAW) method to represented the core and valence electrons with a kinetic

cutoff energy of 400 eV. [8-9] The atomic structures were fully relaxed until energy and forces were converged to 10^{-5} eV $Å^{-1}$ and 0.02 eV $Å^{-1}$, respectively. To overcome the known self-interaction error in DFT and to make the bandgap close to experiment, the DFT+U (Ueff = 6.2 eV, 4.6 eV and 2.4 eV for Ni, Fe and Mo atoms, respectively.) method was used to treat the 3d electrons of the transition metal.[10] A 3×4×1 Monkhorst-Pack k-point mesh was employed to sample the Brillouin zone for all surface model. All calculations were performed on a (001) slab model with 1 × 2 surface cell, containing atomic layers and a vacuum layer of 15 Å thickness to avoid artificial interaction between periodic images. In order to improve the description of van der Waals interaction, DFT-D3 correction was employed.[11]

The OH*, O*, and OOH* adsorption free energy (ΔG_s) on disparate active sites can be defined as equation (1):

$$\Delta G_s = \Delta E_s + \Delta E_{ZPE} - T\Delta S_s \quad (1)$$

Where ΔE_s is the hydrogen absorption energy, ΔE_{ZPE} is the difference in zero point energy between the surface species and dissociative species, T is the temperature (degree kelvin, K), and S_s is the entropy change between the adsorbed state of the system and the gas phase standard state. At this point, the ΔG_s of different sites can be acquired. Vaspkit code is used for post-computation.

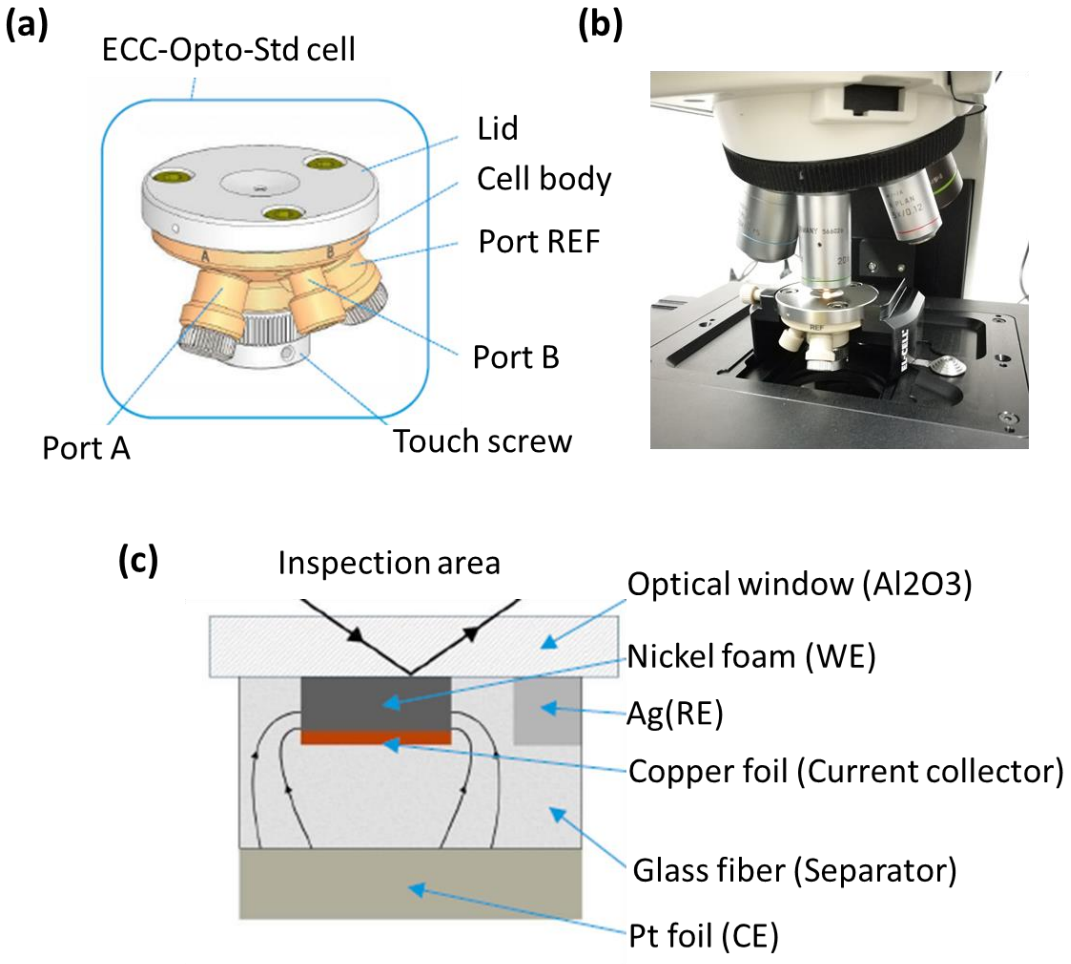

Figure S1 ECC-Opto-Std test cell serves to monitor the optical properties of an electrode material in the course of electrochemical processing. For this purpose, the working electrode (WE) material is placed right below the optical window. Ag foil and Pt foil was used as reference electrode and counter electrode, respectively.

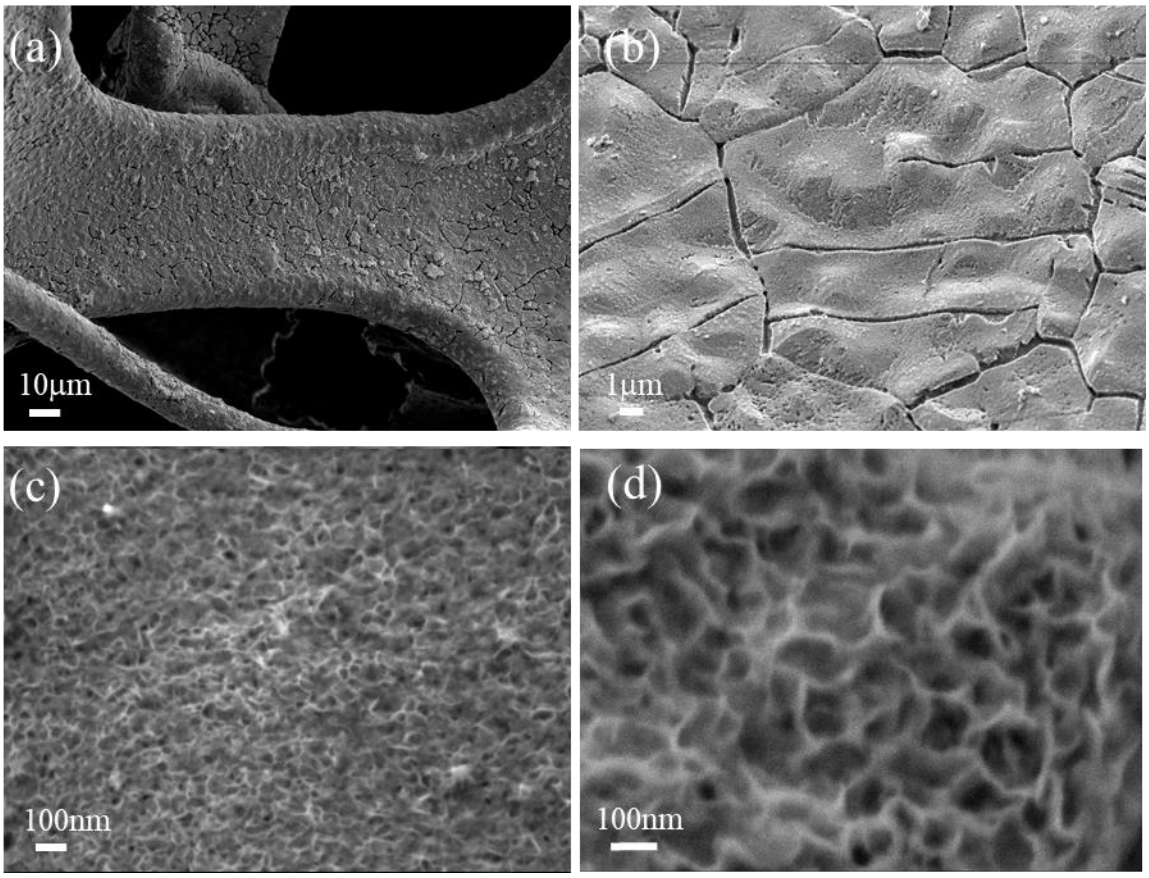

Figure S2. SEM images of NiFe/NF with different magnification.

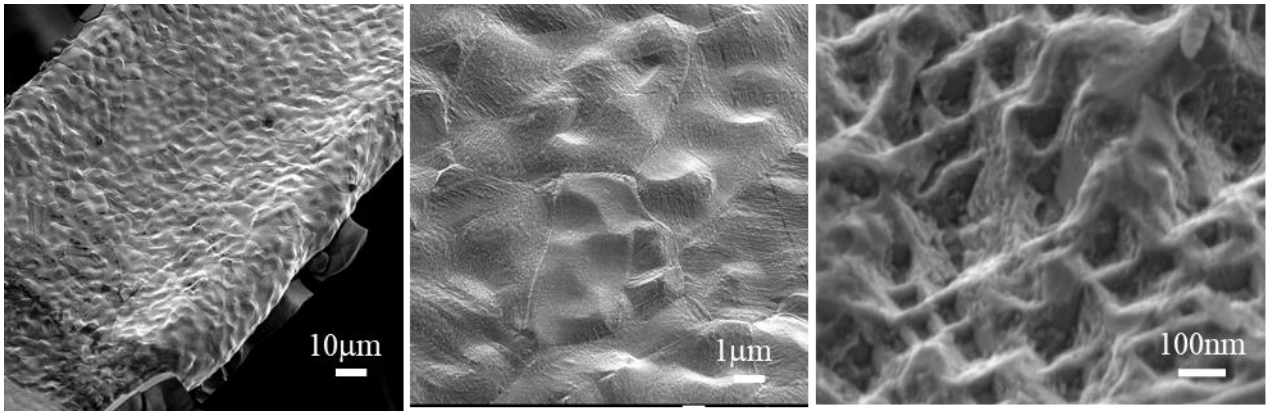

Figure S3. SEM images of NiFeMo/NF with different magnification.

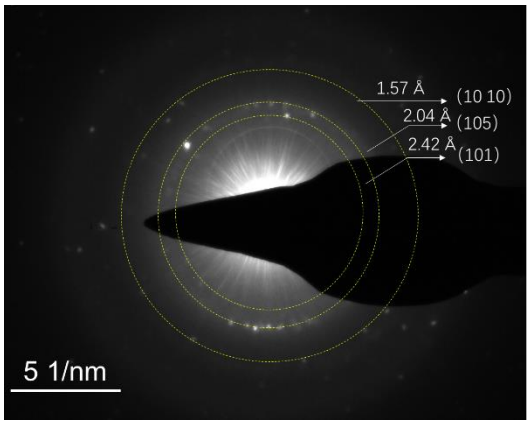

Figure S4 The corresponding SAED pattern in Figure-1(f)

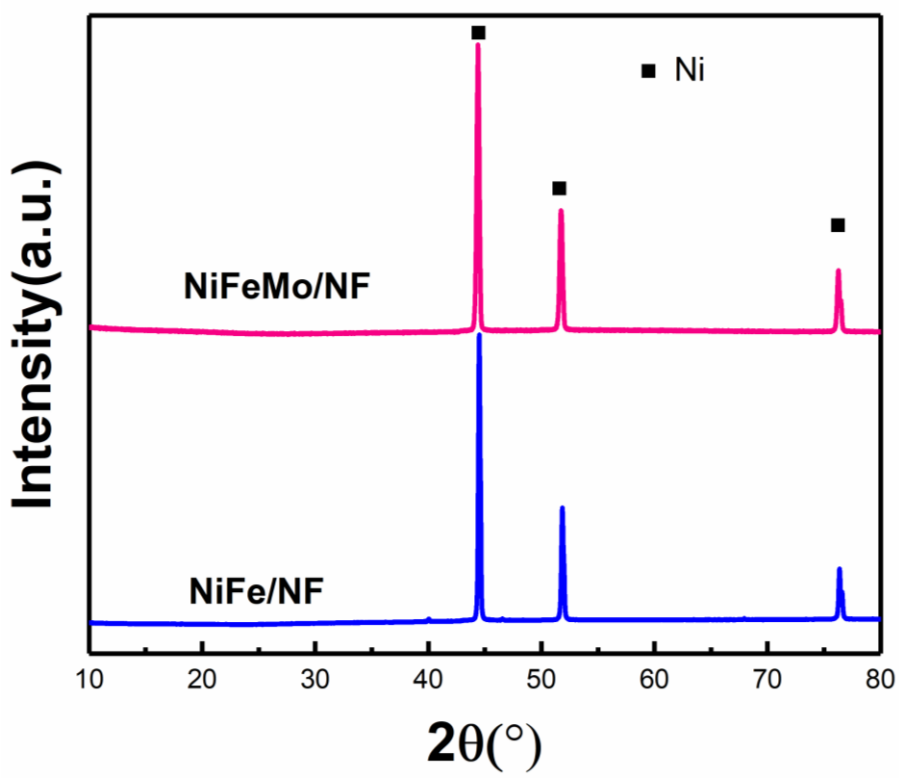

Figure S5 XRD patterns of NiFe/NF and NiFeMo/NF

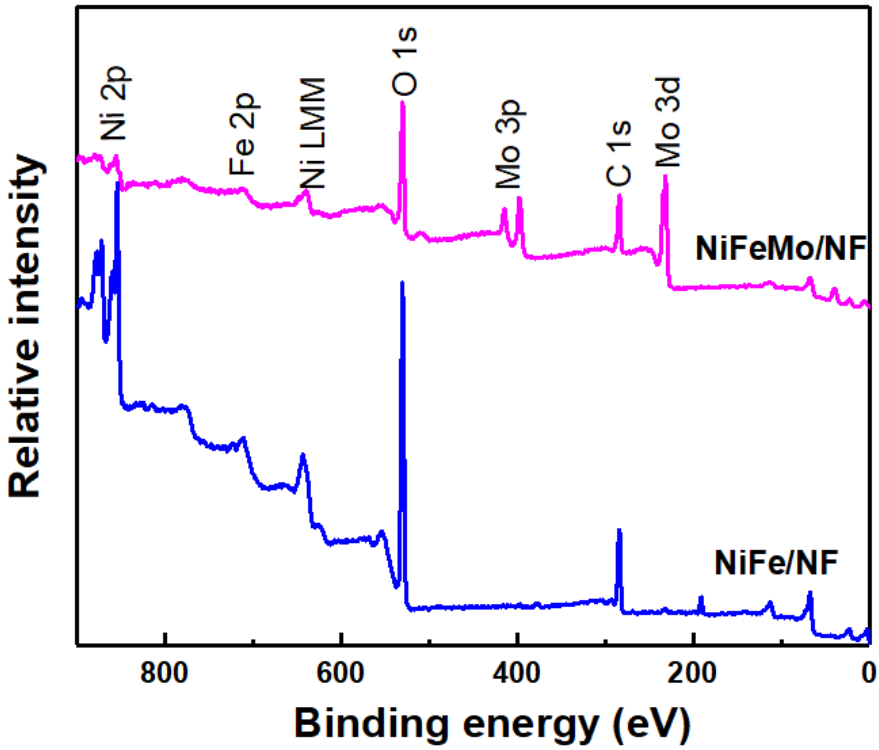

Figure S**6** Survey XPS spectra of NiFe and NiFeMo catalysts.

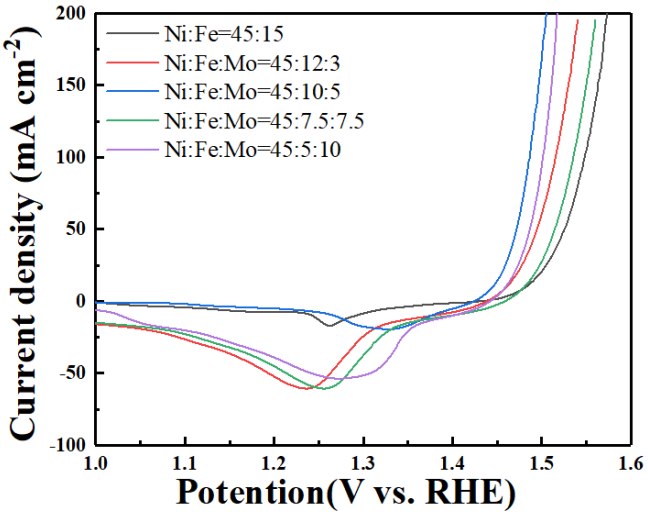

Figure S7 Polarization curves of the NiFeMo/NF catalysts with different raw material feed ratio. When the ratio is 9:2:1 (45:10:5), NiFeMo shows the best performance

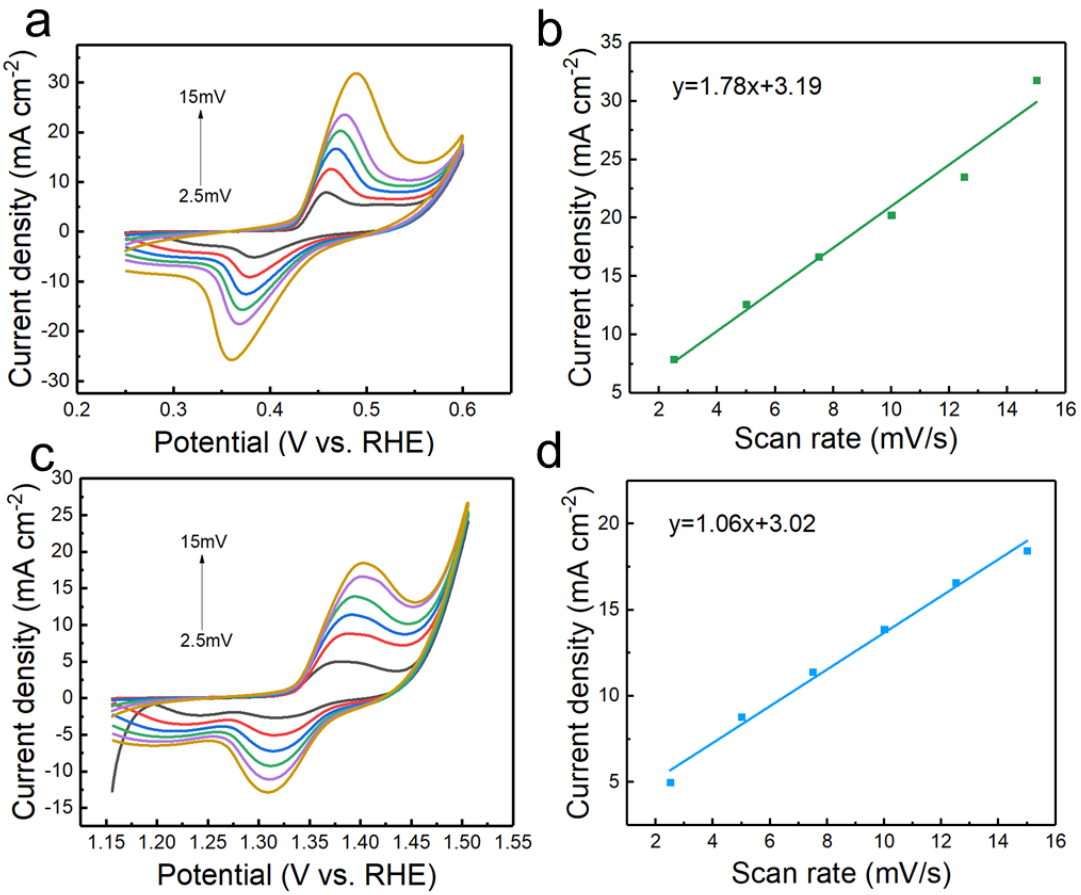

Figure S8 CV scans of Ni redox and the corresponding anodic charging currents as a function of scan rate in (a) and (b) NiFe/NF, as well as (c) and (d) NiFeMo/NF prior to OER.

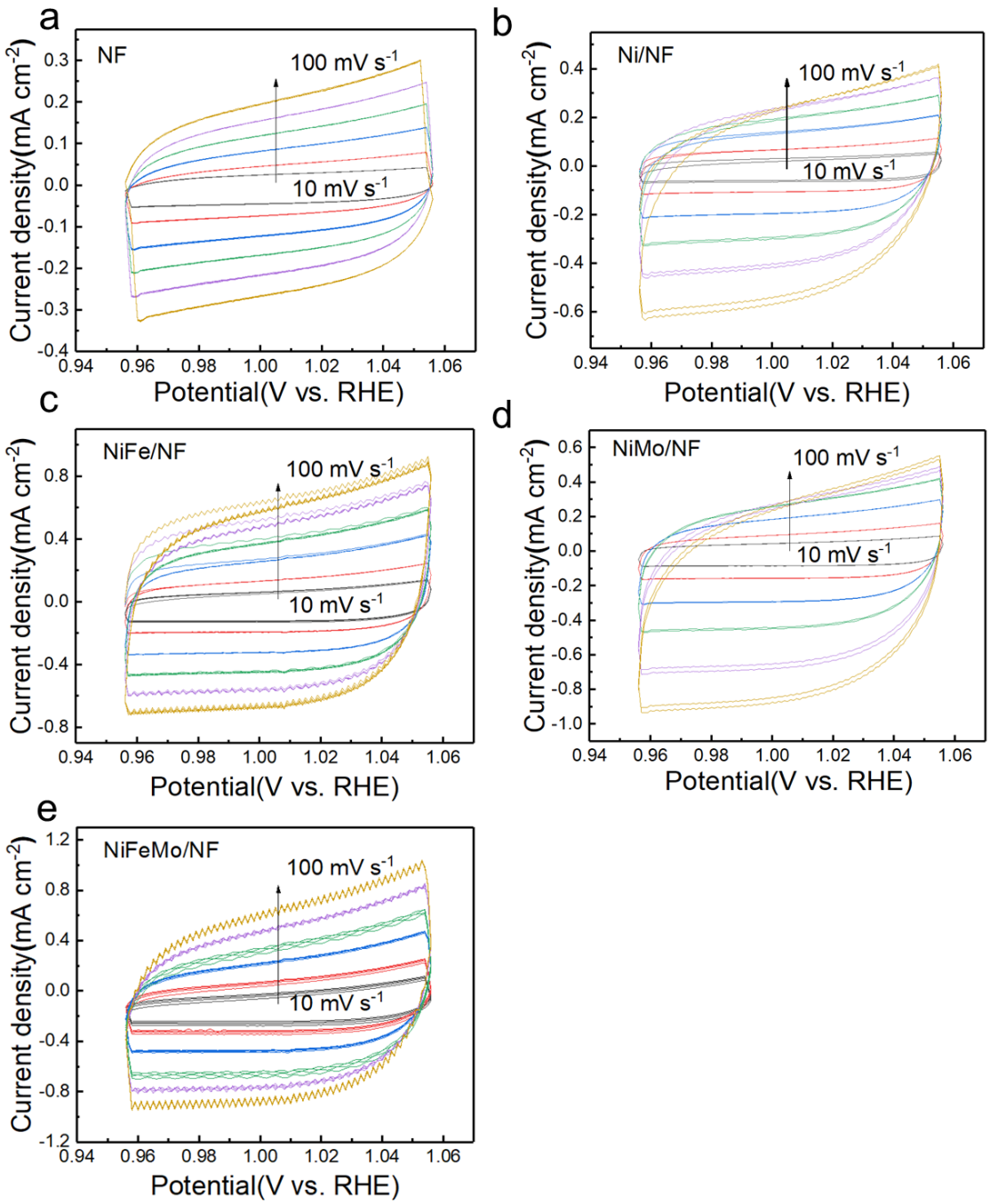

Figure S9 CV curves for different electrocatalysts carried out in non-faradic regions at different scan rates in 1M KOH

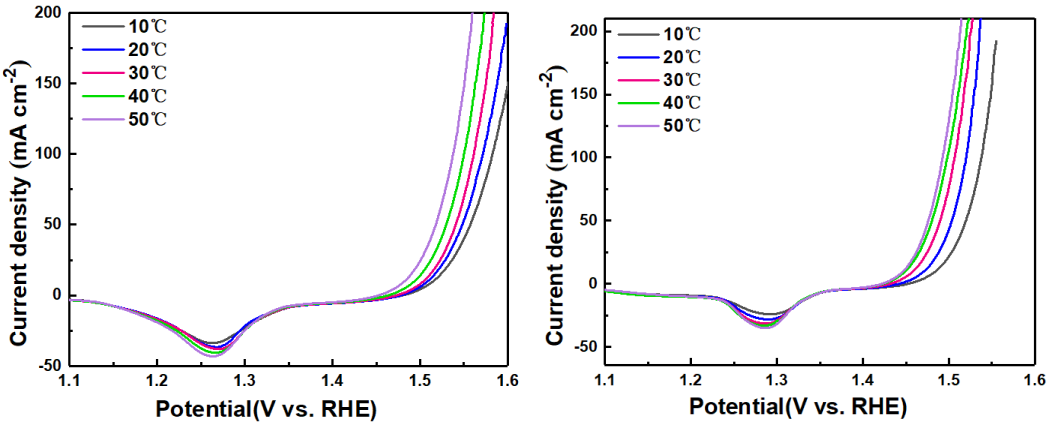

Figure S10 The temperature dependent LSV curves for both (a)NiFe and (b)NiFeMo catalysts.

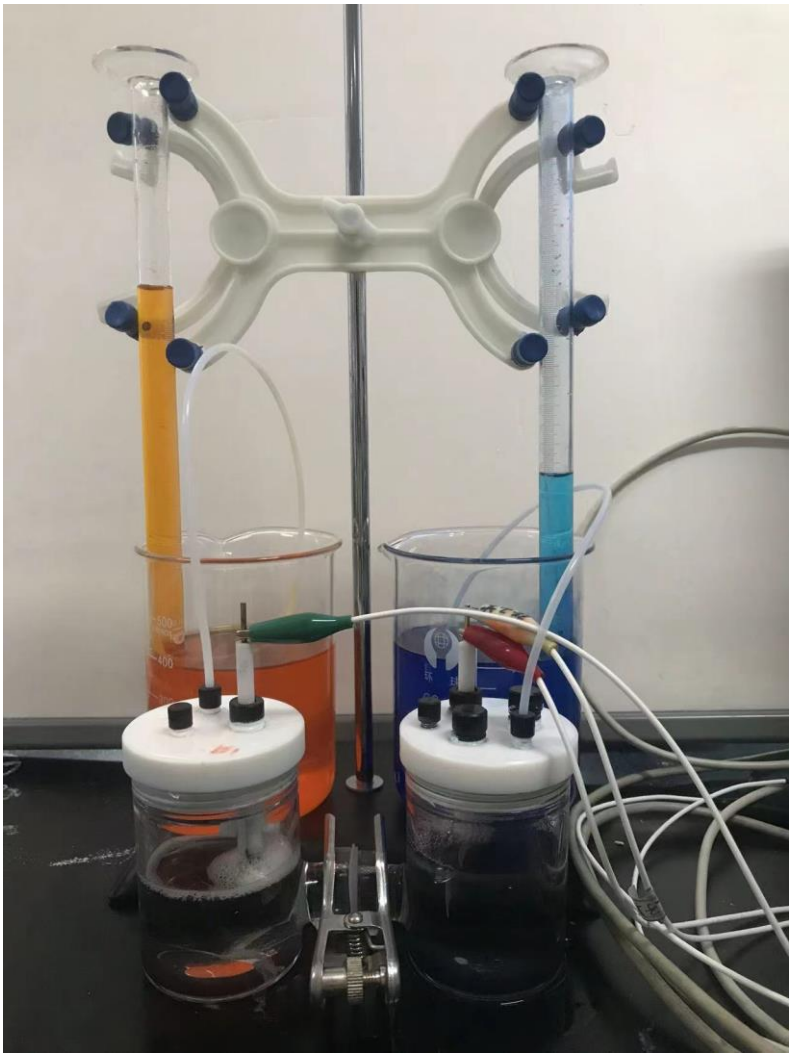

. FigureS11 Faradic efficiency test device.

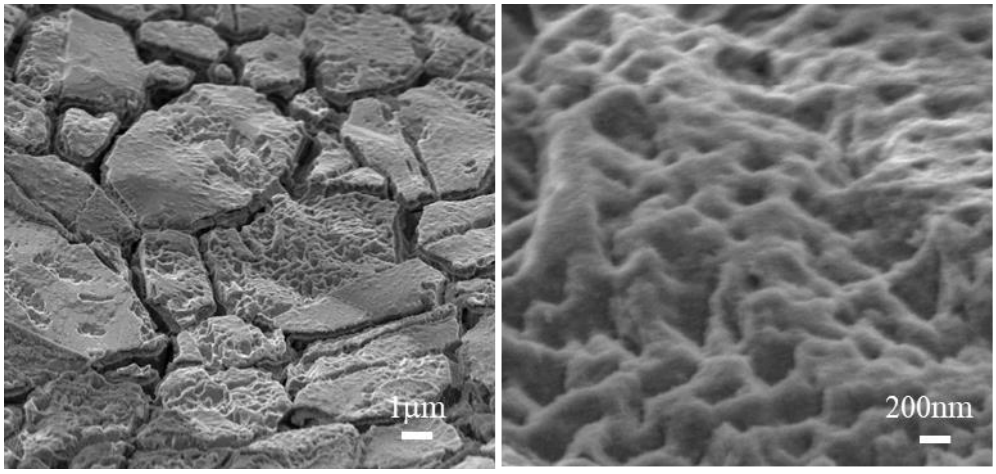

Figure S12 SEM images of NiFeMo/NF after OER stability test for 16.7h with different magnification

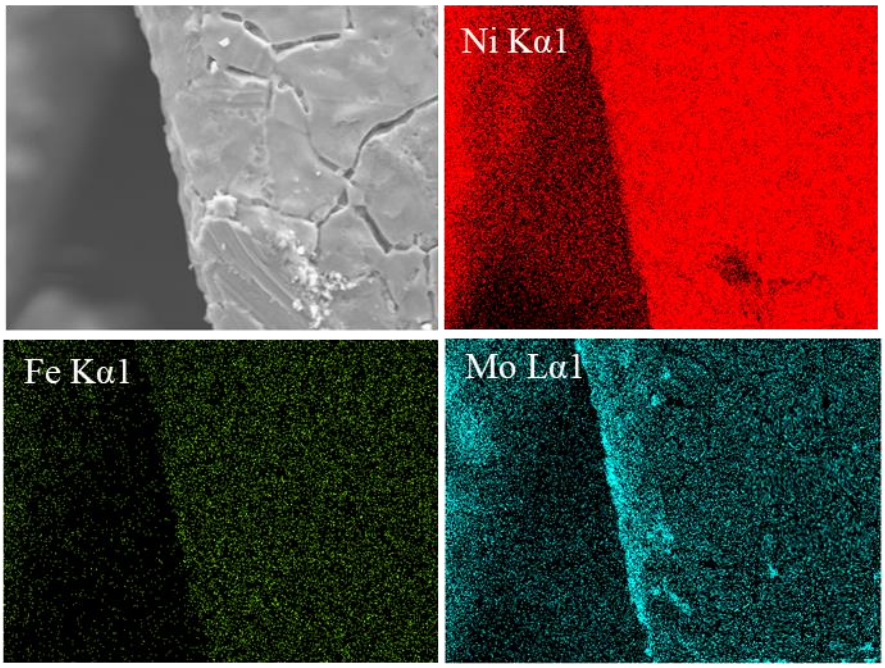

Figure S13. SEM image and corresponding EDX mapping images of the NiFeMo/NF after the OER stability test for 16.7 h..

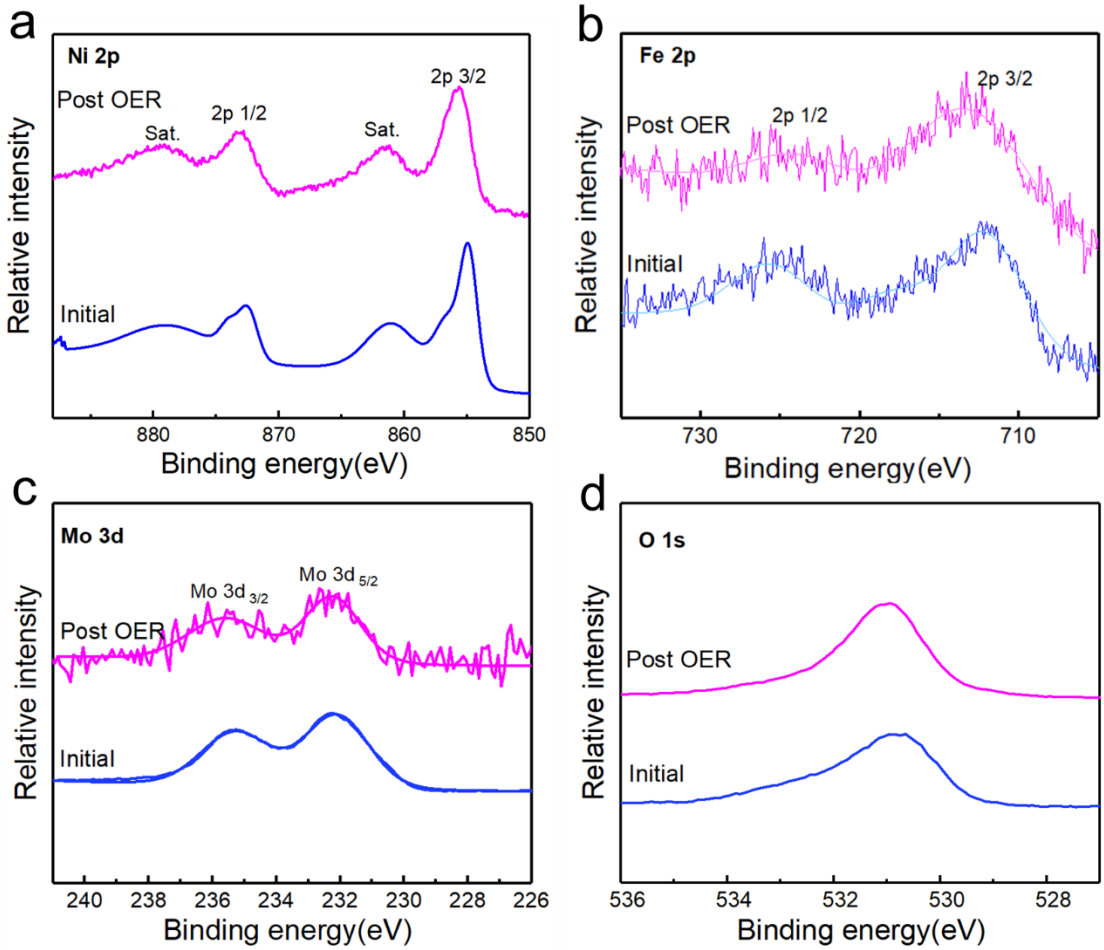

Figure S14 XPS spectra comparison of fresh NiFeMo/NF electrocatalyst and NiFeMo/NF electrocatalysts after the OER stability tests. Ni 2p (a), Fe 2p (b), Mo 3d (c) and O 1s (d).

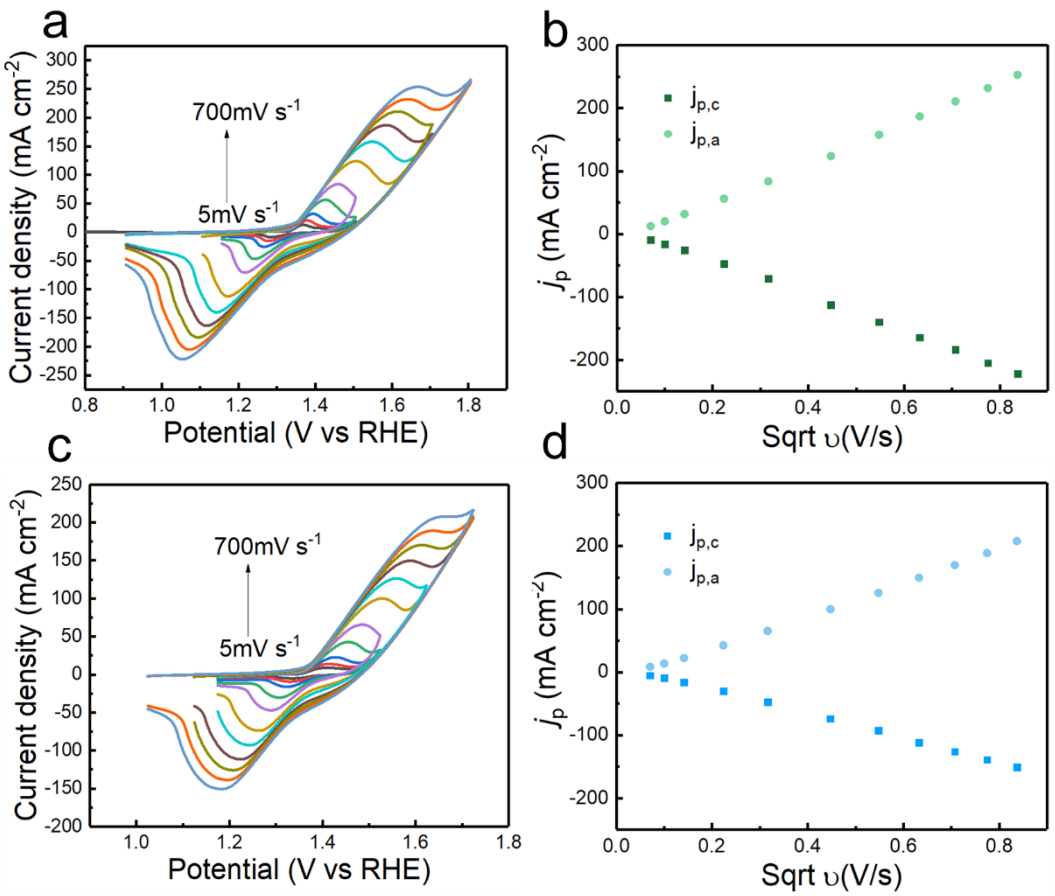

Figure S15. Laviron analysis: variation of Ni redox pair as a function of CV scan rate with 5,10,20,50,100,200,300,400,500,600,700 mV s-1 in (a) NiFe/NF and (c) NiFeMo/NF. The peak current response for Ni redox pair as a function of square root of scan rate in (b)NiFe/NF and (d)NiFeMo/NF.

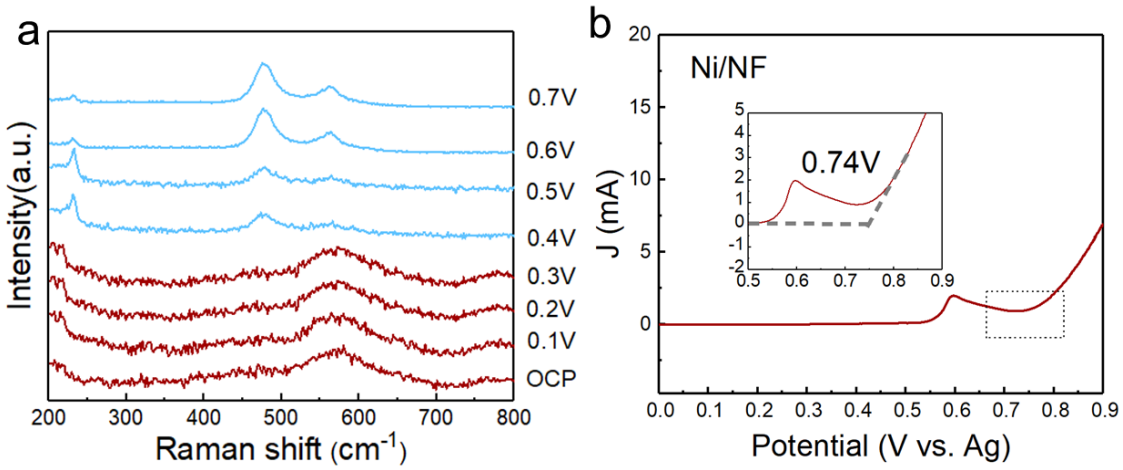

Figure S16 (a) Operando Raman spectra of Ni/NF sample under various potential. (b) The corresponding polarization curves of Ni/NF.

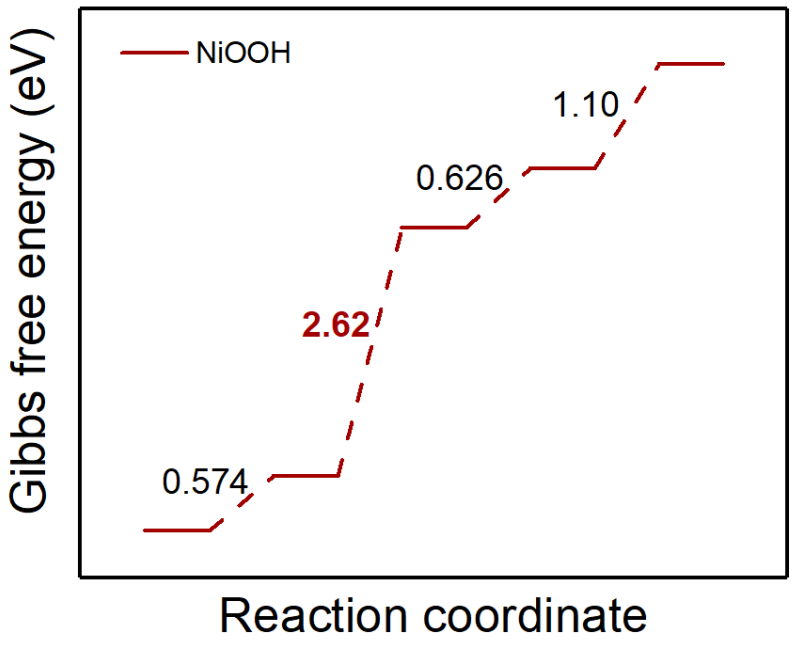

Figure S17 Gibbs free duagram of OER steps on Ni (oxy)hydroxide.

Table S1. Comparison of OER activity of NiFeMo (red words) and recently reported benchmark catalysts.

Catalysts	Support	Electrolyte	J/mA · cm^{-2}	Overpotential/ mV	Tafel/ mV dec^{-1}	Ref.
NiFeMo	NF	1.0 M KOH	10	215	37.9	This work
NiFe	NF	1.0 M KOH	10	250	53.4	This work
Amorphous NiFeMo	NF	1.0 M KOH	10	255	35	[12]
Ce-NiFe LDH	NF	1.0 M KOH	10	205	37.9	[13]
Ta-NiFe LDH	CFP	1.0 M KOH	50	260	58.95	[14]
$Ni_3Fe_{0.5}V_{0.5}$	CFP	1.0 M KOH	100	264	39	[15]
NiFeV-LDHs	NF	1.0 M KOH	10	231	39.4	[16]
NiFeV-LDH	Ni Foam	1.0 M KOH	20	195	42	[17]
NiFeCr	NF	1.0 M KOH	Onset	240	36	[18]
NiFeCr-LDH	CFP	1.0 M KOH	25	225	69	[19]
Mn-doped NiFe-LDH	NF	1.0 M KOH	20	289	47	[20]
NiFeMn-LDH	CFP	1.0 M KOH	100	230	68.6	[21]
$Ni_3FeAl_{0.91}$-LDH@NF	NF	1.0 M KOH	20	304	57	[22]
CoFeCr	GC	1.0 M KOH	10	232	31	[23]
NiFeW	CFP	1.0 M KOH	10	239	36	[24]
La-NiFe LDH	NF	1.0 M KOH	10	340	73.7	[25]
NiFeIr-LDH	GC	1.0 M KOH	20	~213	-	[26]
Gd-NiFe LDH	carbon cloth	1.0 M KOH	10	210	40.9	[27]
NiFeRu-LDH	Ni Foam	1.0 M KOH	10	225	-	[28]

Table S2. Resistance values of various samples at 1.506 V vs. RHE.

Catalysts	R_s / Ω	R_{ct} / Ω
NF	1.440	79.41
Ni/NF	1.152	22.46
NiFe/NF	1.110	1.952
NiMo/NF	1.358	2.046
NiFeMo/NF	1.191	0.615

Table S3. Elemental contributions on NiFe and NiFeMo electrode.

Catalysts	*XPS*	*EDS/atomic percentage*
Ni in NiFe	78%	81%
Fe in NiFe	22%	19%
Ni in NiFeMo	74%	78%
Fe in NiFeMo	11%	10%
Mo in NiFeMo	15%	12%

From XPS fitting, as the Ni^0 on the substrate, Ni content should contribute more than the real content in NiFeMo and NiFe hydroxide thin film.

Refernce

1. Liang, H.; Gandi, A. N.; Anjum, D. H.; Wang, X.; Schwingenschlögl, U.; Alshareef, H. N., Plasma-Assisted Synthesis of NiCoP for Efficient Overall Water Splitting. *Nano Letters* **2016,** *16* (12), 7718-7725.

2. Zhou, M.; Weng, Q.; Zhang, X.; Wang, X.; Xue, Y.; Zeng, X.; Bando, Y.; Golberg, D., In situ electrochemical formation of core–shell nickel–iron disulfide and oxyhydroxide heterostructured catalysts for a stable oxygen evolution reaction and the associated mechanisms. *Journal of Materials Chemistry A* **2017,** *5* (9), 4335-4342.

3. Bo, X.; Li, Y.; Chen, X.; Zhao, C., Operando Raman Spectroscopy Reveals Cr-Induced-Phase Reconstruction of NiFe and CoFe Oxyhydroxides for Enhanced Electrocatalytic Water Oxidation. *Chemistry of Materials* **2020,** *32* (10), 4303-4311.

4. Ge, M.; Hussain, G.; Hibbert, D. B.; Silvester, D. S.; Zhao, C., Ionic Liquid‐based Microchannels for Highly Sensitive and Fast Amperometric Detection of Toxic Gases. *Electroanalysis* **2018,** *31* (1), 66-74.

5. Gunawan, C. A.; Ge, M.; Zhao, C., Robust and versatile ionic liquid microarrays achieved by microcontact printing. *Nature Communications* **2014,** *5* (1).

6. Hacene, M.; Anciaux-Sedrakian, A.; Rozanska, X.; Klahr, D.; Guignon, T.; Fleurat-Lessard, P., Accelerating VASP electronic structure calculations using graphic processing units. *Journal of Computational Chemistry* **2012,** *33* (32), 2581-2589.

7. Hutchinson, M.; Widom, M., VASP on a GPU: Application to exact-exchange calculations of the stability of elemental boron. *Computer Physics Communications* **2012,** *183* (7), 1422-1426.

8. Perdew, J. P.; Burke, K.; Ernzerhof, M., Generalized Gradient Approximation Made Simple. *PHYSICAL REVIEW LETTERS* **1996,** *77* (18), 4.

9. Monkhorst, H. J.; Pack, J. D., Special points for Brillouin-zone integrations. *Physical Review B* **1976,** *13* (12), 5188-5192.

10. Liechtenstein, A. I.; Anisimov, V. I.; Zaanen, J., Density-functional theory and strong interactions: Orbital ordering in Mott-Hubbard insulators. *Physical Review B* **1995,** *52* (8), R5467-R5470.

11. Wang, V.; Xu, N.; Liu, J.-C.; Tang, G.; Geng, W.-T., VASPKIT: A user-friendly interface facilitating high-throughput computing and analysis using VASP code. *Computer Physics Communications* **2021,** *267*.

12. Li, Y. K.; Zhang, G.; Lu, W. T.; Cao, F. F., Amorphous Ni-Fe-Mo Suboxides Coupled with Ni Network as Porous Nanoplate Array on Nickel Foam: A Highly Efficient and Durable Bifunctional Electrode for Overall Water Splitting. *Adv Sci (Weinh)* **2020,** *7* (7), 1902034.

13. Liu, M.; Min, K. A.; Han, B.; Lee, L. Y. S., Interfacing or Doping? Role of Ce in Highly Promoted Water Oxidation of NiFe‐Layered Double Hydroxide. *Advanced Energy Materials* **2021**.

14. Wang, X.; Tuo, Y.; Zhou, Y.; Wang, D.; Wang, S.; Zhang, J., Ta-doping triggered electronic structural engineering and strain effect in NiFe LDH for enhanced water oxidation. *Chemical Engineering Journal* **2021,** *403*.

15. Jiang, J.; Sun, F.; Zhou, S.; Hu, W.; Zhang, H.; Dong, J.; Jiang, Z.; Zhao, J.; Li, J.; Yan, W.; Wang, M., Atomic-level insight into super-efficient electrocatalytic oxygen evolution on iron and vanadium co-doped nickel (oxy)hydroxide. *Nat Commun* **2018,** *9* (1), 2885.

16. Dinh, K. N.; Zheng, P.; Dai, Z.; Zhang, Y.; Dangol, R.; Zheng, Y.; Li, B.; Zong, Y.; Yan, Q., Ultrathin Porous NiFeV Ternary Layer Hydroxide Nanosheets as a Highly Efficient Bifunctional Electrocatalyst for Overall Water Splitting. *Small* **2018,** *14* (8).

17. Li, P.; Duan, X.; Kuang, Y.; Li, Y.; Zhang, G.; Liu, W.; Sun, X., Tuning Electronic Structure of NiFe Layered Double Hydroxides with Vanadium Doping toward High Efficient Electrocatalytic Water Oxidation. *Advanced Energy Materials* **2018,** *8* (15).

18. Bo, X.; Hocking, R. K.; Zhou, S.; Li, Y.; Chen, X.; Zhuang, J.; Du, Y.; Zhao, C., Capturing the active sites of multimetallic (oxy)hydroxides for the oxygen evolution reaction. *Energy & Environmental Science* **2020,** *13* (11), 4225-4237.

19. Yang, Y.; Dang, L.; Shearer, M. J.; Sheng, H.; Li, W.; Chen, J.; Xiao, P.; Zhang, Y.; Hamers, R. J.; Jin, S., Highly Active Trimetallic NiFeCr Layered Double Hydroxide Electrocatalysts for Oxygen Evolution Reaction. *Advanced Energy Materials* **2018,** *8* (15), 1703189.

20. Lu, Z.; Qian, L.; Tian, Y.; Li, Y.; Sun, X.; Duan, X., Ternary NiFeMn layered double hydroxides as highly-efficient oxygen evolution catalysts. *Chemical communications* **2016,** *52* (5), 908-11.

21. Zhou, D.; Cai, Z.; Jia, Y.; Xiong, X.; Xie, Q.; Wang, S.; Zhang, Y.; Liu, W.; Duan, H.; Sun, X., Activating basal plane in NiFe layered double hydroxide by Mn2+ doping for efficient and durable oxygen evolution reaction. *Nanoscale Horizons* **2018**.

22. Liu, H.; Wang, Y.; Lu, X.; Hu, Y.; Zhu, G.; Chen, R.; Ma, L.; Zhu, H.; Tie, Z.; Liu, J.; Jin, Z., The effects of Al substitution and partial dissolution on ultrathin NiFeAl trinary layered double hydroxide nanosheets for oxygen evolution reaction in alkaline solution. *Nano Energy* **2017,** *35*, 350-357.

23. Chen, J.; Li, H.; Chen, S.; Fei, J.; Liu, C.; Yu, Z.; Shin, K.; Liu, Z.; Song, L.; Henkelman, G.; Wei, L.; Chen, Y., Co–Fe–Cr (oxy)Hydroxides as Efficient Oxygen Evolution Reaction Catalysts. *Advanced Energy Materials* **2021,** *11* (11).

24. Ding, L.; Li, K.; Xie, Z.; Yang, G.; Yu, S.; Wang, W.; Yu, H.; Baxter, J.; Meyer, H. M.; Cullen, D. A.; Zhang, F.-Y., Constructing Ultrathin W-Doped NiFe Nanosheets via Facile Electrosynthesis as Bifunctional Electrocatalysts for Efficient Water Splitting. *ACS Applied Materials & Interfaces* **2021,** *13* (17), 20070-20080.

25. Yu, J.; Lu, K.; Wang, C.; Wang, Z.; Fan, C.; Bai, G.; Wang, G.; Yu, F., Modification of NiFe Layered Double Hydroxide by Lanthanum Doping for Boosting Water Splitting. *Electrochimica Acta* **2021**.

26. Chen, Q. Q.; Hou, C. C.; Wang, C. J.; Yang, X.; Shi, R.; Chen, Y., Ir(4+)-Doped NiFe LDH to expedite hydrogen evolution kinetics as a Pt-like electrocatalyst for water splitting. *Chem Commun (Camb)* **2018,** *54* (49), 6400-6403.

27. Li, M.; Li, H.; Jiang, X.; Jiang, M.; Zhan, X.; Fu, G.; Lee, J.-M.; Tang, Y., Gd-induced electronic structure engineering of a NiFe-layered double hydroxide for efficient oxygen evolution. *Journal of Materials Chemistry A* **2021,** *9* (5), 2999-3006.

28. Chen, G.; Wang, T.; Zhang, J.; Liu, P.; Sun, H.; Zhuang, X.; Chen, M.; Feng, X., Accelerated Hydrogen Evolution Kinetics on NiFe-Layered Double Hydroxide Electrocatalysts by Tailoring Water Dissociation Active Sites. *Advanced materials* **2018,** *30* (10).